DOI: 10.1002/chem.200700750

A New Generation of Metal String Complexes: Structure, Magnetism, Spectroscopy, Theoretical Analysis, and Single Molecular Conductance of an Unusual Mixed-Valence Linear $[Ni_5]^{8+}$ Complex

Isiah Po-Chun Liu,[a, b] Marc Bénard,*[c] Hasan Hasanov,[a] I-Wen Peter Chen,[d] Wei-Hsiang Tseng,[d] Ming-Dung Fu,[d] Marie-Madeleine Rohmer,[c] Chun-hsien Chen,[a, d] Gene-Hsiang Lee,[a] and Shie-Ming Peng*[a, b]

Abstract: Two new linear pentanickel complexes $[Ni_5(bna)_4(Cl)_2][PF_6]_2$ (**1**) and $[Ni_5(bna)_4(Cl)_2][PF_6]_4$ (**2**; bna = binaphthyridylamide), were synthesized and structurally characterized. A derivative of **1**, $[Ni_5(bna)_4(NCS)_2][NCS]_2$ (**3**), was also isolated for the purpose of the conductance experiments carried out in comparison with $[Ni_5(tpda)_4(NCS)_2]$ (**4**; tpda = tripyridyldiamide). The metal framework of complex **2** is a standard $[Ni_5]^{10+}$ core, isoelectronic with that of $[Ni_5(tpda)_4Cl_2]$ (**5**). Also as in **5**, complex **2** has an antiferromagnetic ground state ($J = -15.86\ cm^{-1}$) resulting from a coupling between the terminal nickel atoms, both in high-spin sate ($S = 1$). Complex **1** displays the first characterized linear nickel framework in which the usual sequence of Ni^{II} atoms has been *reduced* by two electrons. Each dinickel unit attached to the naphthyridyl moieties is assumed to undergo a one-electron reduction, whereas the central nickel formally remains Ni^{II}. DFT calculations suggest that the metal framework of the mixed-valence complex **1** should be described as intermediate between a localized picture corresponding to Ni^{II}-Ni^{I}-Ni^{II}-Ni^{I}-Ni^{II} and a fully delocalized model represented as $(Ni_2)^{3+}$-Ni^{II}-$(Ni_2)^{3+}$. Assuming the latter model, the ground state of **1** results from an antiferromagnetic coupling ($J = -34.03\ cm^{-1}$) between the two $(Ni_2)^{3+}$ fragments, considered each as a single magnetic centre ($S = 3/2$). An intervalence charge-transfer band is observed in the NIR spectrum of **1** at 1186 nm, suggesting, in accordance with DFT calculations, that **1** should be assigned to Robin–Day class II of mixed-valent complexes. Scanning tunnelling microscopy (STM) methodology was used to assess the conductance of single molecules of **3** and **4**. Compound **3** was found ≈40% more conductive than **4**, a result that could be assigned to the electron mobility induced by mixed-valency in the naphthyridyl fragments.

Keywords: density functional calculations · electron transport · magnetic properties · metal–metal interactions · mixed-valent compounds · molecular wires

Introduction

The research interest toward extended metal-atom chains (EMACs) based on polypyridylamido ligands has increased significantly in recent years, fuelled by the potential applications of 1D nano-objects in quantum electronics.[1–3] In this field, a number of tri-, tetra-, penta-, hepta-, and nanonuclear complexes have been synthesized and characterized in the group of Cotton and Murillo, in our group, and elsewhere.[4] The structural, magnetic, and spectroscopic properties of these metal strings have been the object of intensive investigation.[5–7] Besides experimental discussions, Rohmer et al. have reported DFT calculations on these complexes, providing some hints to clarify the electronic configurations of polypyridylamide-based EMACs and their influence on structural and magnetic properties.[8] Other thorough investi-

[a] I. P.-C. Liu, Dr. H. Hasanov, Prof. C.-h. Chen, Dr. G.-H. Lee, Prof. S.-M. Peng
Department of Chemistry, National Taiwan University
1, Roosevelt Rd., Sec. 4, Taipei 106 (Taiwan)
Fax: (+886) 2-8369-3765
E-mail: smpeng@ntu.edu.tw

[b] I. P.-C. Liu, Prof. S.-M. Peng
Institute of Chemistry, Academia Sinica
Taipei 115 (Taiwan)

[c] Dr. M. Bénard, Dr. M.-M. Rohmer
Laboratoire de Chimie Quantique, Institut de Chimie
UMR 7177, 4, rue Blaise Pascal, 67000 Strasbourg (France)
Fax: (+33) 390-241-301
E-mail: benard@quantix.u-strasbg.fr

[d] I.-W. P. Chen, W.-H. Tseng, M.-D. Fu, Prof. C.-h. Chen
Department of Chemistry, National Tsing Hua University
Hsinchu 30013 (Taiwan)

Supporting information for this article is available on the WWW under http://www.chemeurj.org/ or from the author.

gations on these complexes have been recently carried out by Pantazis and McGrady,[9] and by Kitagawa et al.[10]

Recent investigations conducted in our group to assess the relative conductivity of single metal string molecules by means of scanning tunnelling microcopy (STM) have shown that nickel strings seem to be slightly less conductive than their cobalt and chromium analogues.[3a,c] It was proposed that the relatively low conductivity of polynickel EMACs is related to the weakness of the delocalized bonding along the metal string. Nickel, however, remains a metal of great interest in view of the facile synthesis of Ni-based metal strings and because of the high yields that are currently obtained, relative to other metals. Therefore, one of the research goals pursued in our group is the design of advanced polynuclear metal strings combining a high synthesis yield with a good conductivity. A possible strategy for approaching this goal is the characterization of mixed-valence (MV) complexes, especially those in which unpaired electrons are expected to move easily along the metal chain. According to the Robin–Day classification of MV complexes, the molecules most interesting should belong, a priori, either to class III (electron-delocalized) or to class II (displaying some electron delocalization).[11] The corresponding materials are expected to be conductors (class III), or semiconductors (class II), while class I MV complexes are insulators.[12]

Among the currently available dimetallic MV compounds ascribed as conductors, the series $[Ni_2(napy)_4(X)_2][BPh_4]$ (napy = 1,8-naphthyridine; X = Cl, Br, I), characterized by the presence of three delocalized electrons in the dinickel core,[13,14] could represent a good candidate for the synthesis of a conducting metal wire (Schemes 1 and 2). The coupling of 1,8-naphthyridine molecules with amino groups could therefore provide an alternative to polypyridylamide ligands for the synthesis of polynickel wires based on dinuclear mixed-valence elements (Scheme 2). The binaphthyridylamide (bna) ligand was obtained according to the procedure shown in Scheme 3, and then used to synthesize the pentanickel complex $[Ni_5(bna)_4(Cl)_2][PF_6]_2$ (**1**), containing two $(Ni_2)^{3+}$ units separated with one Ni^{II} atom. Complex **1** could then be oxidized into $[Ni_5(bna)_4(Cl)_2][PF_6]_4$ (**2**), in which all metal atoms can be formally described as Ni^{II}. Crystallographic characterization, magnetic susceptibility measurements and DFT calculations are reported for these two new pentanickel complexes, in view of their potential for the development of a new family of EMACs with improved conductive properties.[3] In order to assess these conductive potentialities, a derivative of **1**, $[Ni_5(bna)_4(NCS)_2][NCS]_2$ (**3**), was isolated successfully and its conductivity was measured by means of STM techniques, in comparison with $[Ni_5(tpda)_4(NCS)_2]$, **4**.

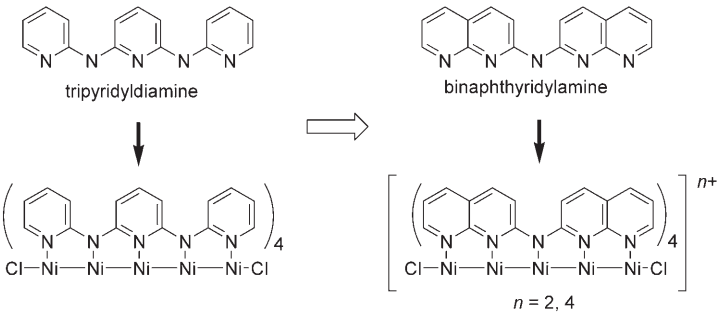

Scheme 2.

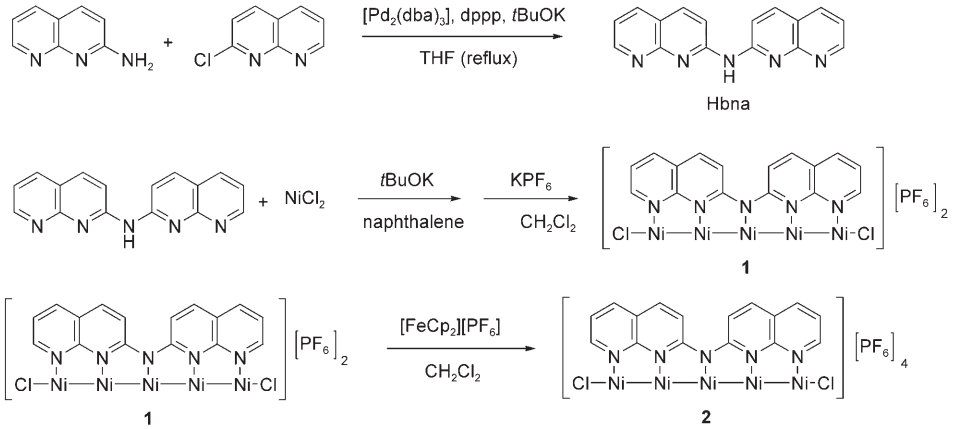

Scheme 3. Synthesis of complexes **1** and **2**.

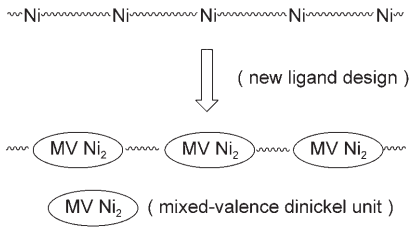

Scheme 1. The ideal strategy for designing new polynickel wires.

Results and Discussion

Synthesis: The overall synthetic routes to the bna ligand, and then to complexes **1** and **2** are summarized in Scheme 3. The Hbna ligand was prepared by reaction of 2-amino-1,8-naphthyridine and 2-chloro-1,8-naphthyridine with palladium catalyst. Treatment of Hbna with $NiCl_2$ in the presence of *t*BuOK, followed by excess of KPF_6, generated compound **1**. The two-electron oxidation leading to product **2** was obtained by reacting **1** with $[Cp_2Fe][PF_6]$ in CH_2Cl_2.

X-ray characterization: The crystallographic data for **1** and **2** are reported in Table 1, and labelled ORTEP plots excluding solvent molecules are displayed in Figure 1.

Table 1. X-ray crystallographic data for **1** and **2**.

	1·6 CH_2Cl_2	**2**·4 CH_3CN·2 Et_2O
formula	$C_{70}H_{52}Cl_{14}F_{12}N_{20}Ni_5P_2$	$C_{80}H_{72}Cl_2F_{24}N_{24}Ni_5O_2P_4$
M_r	2253.11	2345.95
crystal system	monoclinic	orthorhombic
space group	*C*2/*c*	*Pbcn*
a [Å]	25.4608(9)	28.7086(5)
b [Å]	15.2805(6)	13.5487(2)
c [Å]	20.7850(8)	23.6078(4)
α [°]	90	90
β [°]	91.945(2)	90
γ [°]	90	90
V [Å^3]	8081.8(5)	9182.6(3)
Z	4	4
T [K]	150(1)	150(1)
ρ_{calcd} [g cm^{-3}]	1.852	1.697
$R1$[a]/$wR2$[b] [$I > 2\sigma(I)$]	0.0868/0.2386	0.0620/0.1767
$R1$[a]/$wR2$[b] (all data)	0.1881/0.2975	0.1122/0.1982

[a] $R1 = \Sigma|F_o| - |F_c|/\Sigma|F_o|$. [b] $wR2 = [\Sigma[w(F_o^2 - F_c^2)^2]/\Sigma[w(F_o^2)^2]]^{1/2}$, in which $w = 1/\sigma^2(F_o^2) + (aP)^2 + bP$, $P = (F_o^2 + 2F_c^2)/3$.

Selected bond lengths observed for both complexes, and for $[Ni_5(tpda)_4Cl_2]$ (**5**), are reported in Figure 2, together with the corresponding values obtained from DFT optimization. The nonplanarity of the bna ligand induces a torsion angle between Ni1–N1 and Ni3–N3 close to 35° for **1** and 38° for **2** (Figure 1). In both cases, the linear pentanickel chain is helically bridged by four bna ligands, and the molecules display approximate D_4 symmetry.

As for **5**, the coordination environments of the three inner Ni atoms are distorted square planar, whereas the two terminal ones are roughly square pyramidal. The trends observed for the bond lengths of **2** are reminiscent of those previously obtained for the other $[Ni_5]^{10+}$ complex **5**,[1,15,16] namely 1) an external Ni–Ni distance close to 2.40 Å and an internal metal–metal distance shorter by ≈0.10 Å, and 2) long metal–nitrogen distances originating at the outermost Ni atoms (≈2.10 Å) compared with much shorter Ni–N distances at all other metal atoms.[17] However, complex **2** displays some specific structural characters: 1) a significantly shorter Ni–Cl distance (2.308 vs. 2.346 Å for **5**) due to the stronger electrostatic attraction between chlorine and the tetracationic complex; and 2) a progressive contraction of the Ni–N bond lengths from the long outermost Ni1–N distance (av 2.095 Å) to the very short distances originating at the central Ni atom (1.867 Å), associated in **2** with the Ni–N bonds involving the most basic amino groups. The two-electron reduction giving rise to complex **1** appreciably modifies these structural characters. The whole coordination environment has expanded, partly due to the decrease of the positive charge of the metal framework, but also because of the presence of two extra electrons to be accommodated on molecular orbitals (MOs) with metal–nitrogen antibonding character. Both effects cumulate to induce an elongation of ≈0.10 Å of the intermediate Ni(2)–N bond lengths (Figure 2). At variance with the metal–ligand bond lengths, the outermost Ni1–Ni2 distances contract from 2.408 to 2.325 Å. This makes the outer metal–metal distances shorter than the internal ones, a structural feature still unprecedented for pentanuclear metal string complexes (M = Co, Ni).[4]

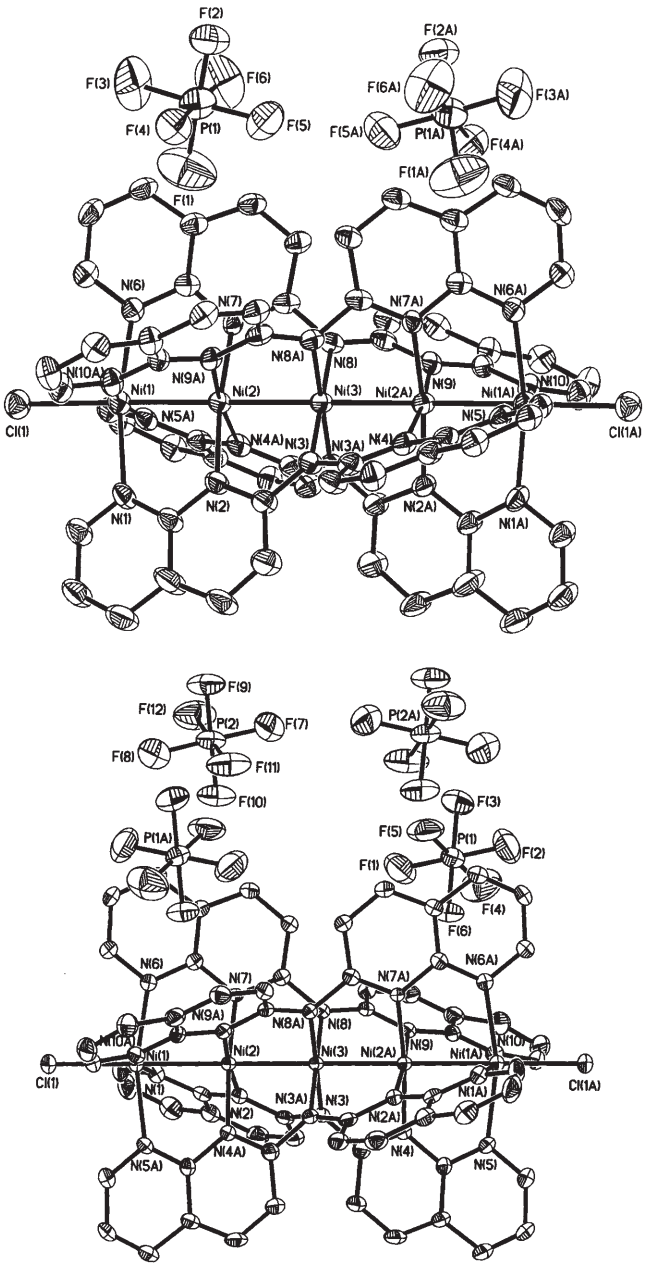

Figure 1. Molecular structures of complexes **1** (top) and **2** (bottom). Ellipsoids are drawn at 30% (top) and at 50% (bottom) probability levels. Hydrogen atoms and interstitial solvents have been omitted for clarity.

Magnetic properties: The magnetic susceptibility of polycrystalline powder samples of **1** and **2** was measured in the

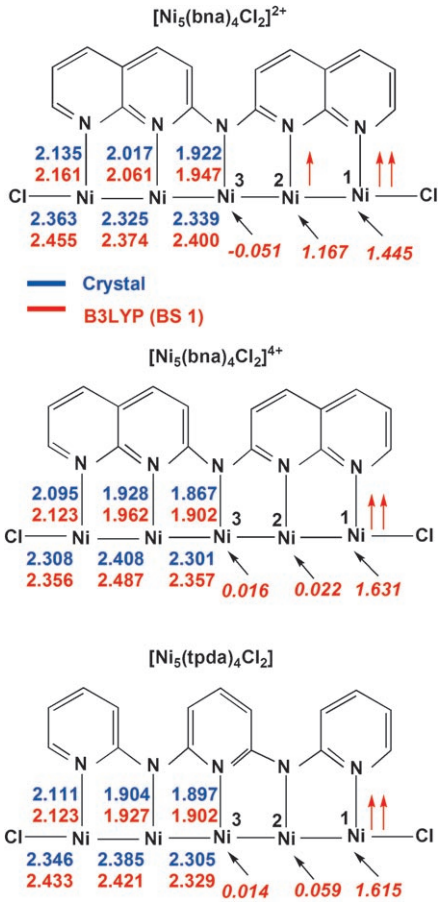

Figure 2. Selected interatomic distances observed (blue) and computed (UB3LYP calculations, red) for **1**, **2**, and **5**. Atomic spin densities computed on the nickel atoms (UB3LYP) are indicated in italics.

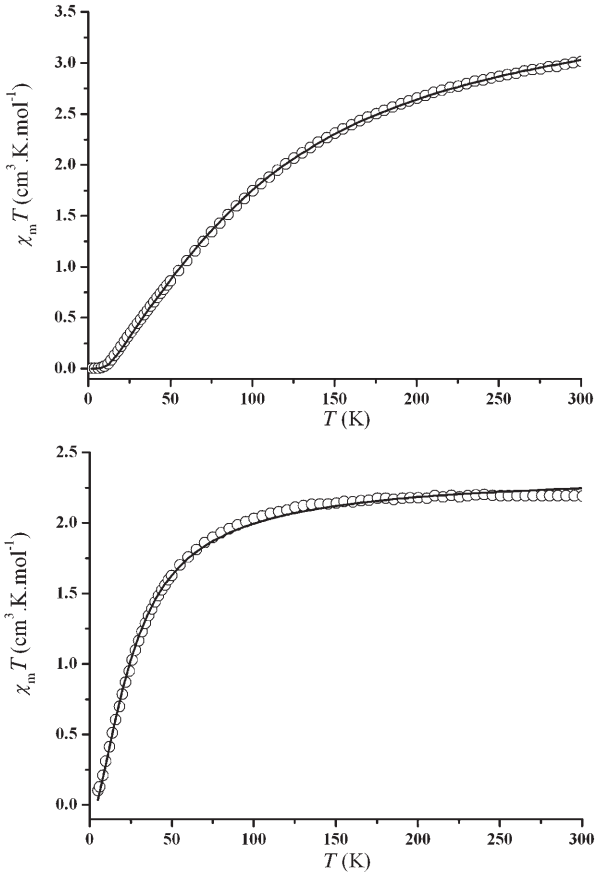

Figure 3. Plot of $\chi_m T$ versus T for complexes **1** (top) and **2** (bottom). The solid line represents the best theoretical fit.

range 4–300 K. The corresponding variations of $\chi_m T$ are reported in Figure 3. For complex **2**, the plot of $\chi_m T$ versus T is similar to that of $[Ni_5]^{10+}$ analogues with two antiferromagnetically coupled high-spin terminal Ni^{II} ions.[1,15,16] Assuming an isotropic interaction between two magnetic centres S_1 and S_2, and accounting for the Zeeman splitting, the usual Heisenberg–Dirac–van Vleck Hamiltonian[18] can be written as Equation (1).

$$\hat{H} = -JS_1 \cdot S_2 + g\beta S \cdot H \quad (1)$$

The temperature-dependant magnetic susceptibility curve could be satisfactorily reproduced ($R^2 = 0.9978$; solid line in Figure 3, bottom) with the development of the van Vleck equation appropriate to $S_1 = S_2 = 1$,[19] associated with the parameters $g = 2.17$ and $J = -15.86\ cm^{-1}$. The J value obtained for **2** appears somewhat smaller than that obtained for $[Ni_5(tpda)_4Cl_2]$ ($J = -33.5\ cm^{-1}$).[1]

The reduced complex **1** displays a $\chi_m T$ value of $3.01\ cm^3 K mol^{-1}$ at 300 K, rapidly decreasing with temperature (Figure 3, top). This value, significantly larger than those obtained in the pentanickel homologues **2** and **5**, clearly points to the presence of extra unpaired electrons in **1**. The short Ni–N distances observed around Ni(3) (1.922 Å) suggest that this atom, with its square-planar environment, retains a low-spin d^8 electronic state. The magnetic susceptibility curve could therefore be interpreted as resulting from the antiferromagnetic interaction between two mixed-valence $[Ni_2]^{3+}$ units separated by the central Ni(3) atom. A model for the individual $[Ni_2]^{3+}$ units is provided by the binuclear $[Ni_2(napy)_4(X)_2]^+$ complexes (napy = 1,8-naphthyridine; X = Cl, Br, I) investigated experimentally and theoretically by Bencini, Gatteschi, et al.[13,14] The symmetric structure of the bromide, and as far as the Ni–N distances are concerned, of the iodide complexes suggests that these formally Ni^{II}–Ni^{I} species belong to class III (delocalized) of the classification of Robin and Day. The ground state of both molecules was found to be a quartet ($S = 3/2$) with no evidence of thermally populated doublets. The high-spin ground state was assigned to the double exchange mechanism, due to the rapid hopping of an extra electron between two integer valence-localized centres.[20] The electron-transfer parameter associated with this process was indeed found from DFT calculations to overcome the opposite effect of the antiferromagnetic coupling between the two Ni atoms.[14] The question is raised of whether the conclusions obtained

by Bencini et al. for $[Ni_2(napy)_4(X)_2]^+$ can be transposed to the dinickel naphthyridyl moieties of complex **1**. It should be noted that the structural similarity between the dinickel monomer and the fragments of **1** is impaired by the nonsymmetric environment along the metal axis. This asymmetry extends to the equatorial environment with a stretching of the outermost Ni(1)–N distances by 0.12 Å with respect to Ni(2)–N (Figure 2), when all Ni–N distances in $[Ni_2(napy)_4(X)_2]^+$ are intermediate at ≈2.09 Å.[14] This structural feature suggests that the delocalization of the spin density is not so complete as in the dinuclear complex. The spin distributions obtained from DFT calculations on **1** confirm that Ni(1) and Ni(2) are not magnetically equivalent (Figure 2) and suggest a model intermediate between the complete delocalization observed in $[Ni_2(napy)_4(X)_2]^+$ and the localized picture displayed in Scheme 4 (top and middle).

However, various attempts to fit the $\chi_m T$ curve within the localized model of Scheme 4 (top and middle) proved unsuccessful. We therefore turned to the delocalized model of Scheme 4 (bottom) and assigned a high-spin ($S=\pm 3/2$) state for both dimetallic fragments considered as comprehensive magnetic entities.

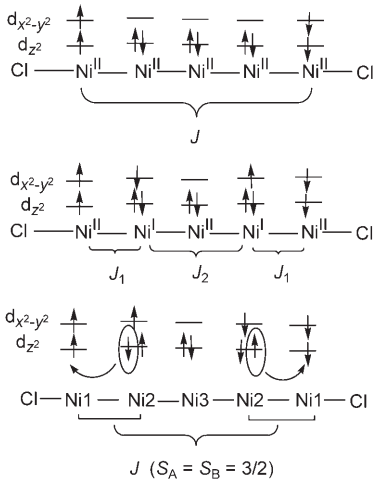

Scheme 4. Top: Coupling scheme for complexes **2** and **5**. Middle: Localized coupling scheme for complex **1**. Bottom: Delocalized coupling scheme for complex **1**.

This model yields a theoretical value of 3.75 $cm^3 K mol^{-1}$ for $\chi_m T$, which is compatible with the value of 3.01 $cm^3 K mol^{-1}$ observed at room temperature for the antiferromagnetically coupled complex. To keep the problem tractable, each $[Ni_2]^{3+}$ unit was considered as a single magnetic centre with $S=3/2$, thus providing, by means of Equation (1) and of the appropriate van Vleck equation,[19] a convenient fit of the experimental susceptibility curve (solid line in Figure 3, top, $R^2=0.9999$) with the set of parameters $g=2.01$ and $J=-34.03$ cm^{-1}.

NMR spectroscopy: The ^{1}H NMR spectra of complexes **1** and **2** in CD_3CN are displayed in Figure 4. Both spectra display five peaks, four of which are in equal integration ratio.[21] This appears to be consistent with the idealized D_4 symmetry assumed for both compounds. Attempts to assign the peaks in both spectra by means of ^{1}H 2D COSY experiments were unsuccessful, due to the lack of resolution. Assignments reported in Figure 4 are therefore proposed on qualitative grounds. Spin density is conveyed to the ligand mainly through the partly occupied $d_{x^2-y^2}$ metal orbitals. This delocalization of the spin density toward the ligand—σ delocalization—induces a downfield shift for the protons of **1** and **2** relative to the protons of the free ligand. The dipole effect, corresponding to a through-space donation from the unpaired electron accommodated on the d_{z^2} orbitals, can be neglected in the first approximation.[22]

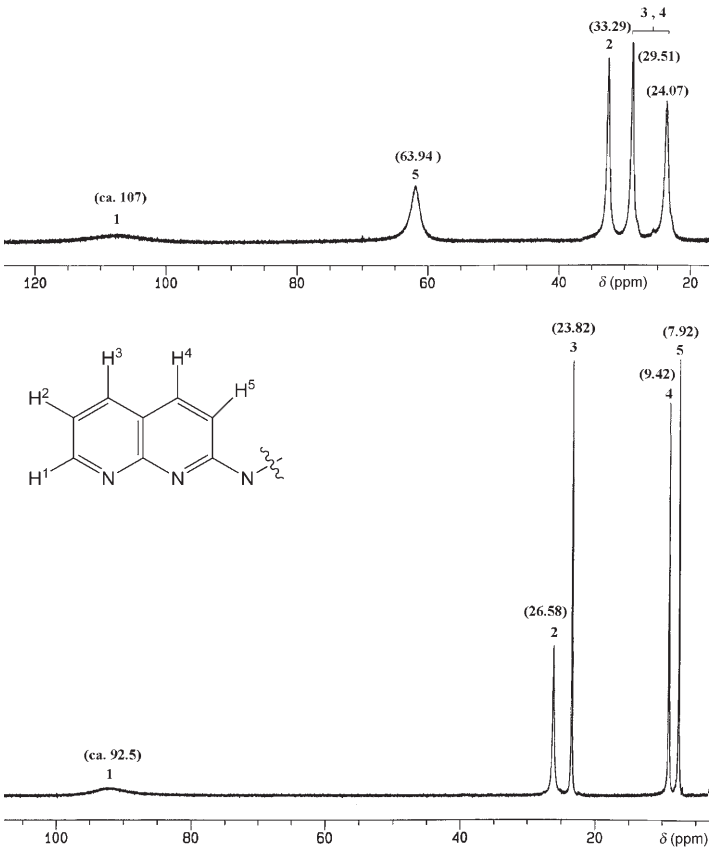

Figure 4. ^{1}H NMR spectrum of **1** (top) and **2** (bottom) in CD_3CN. Chemical shifts are indicated in parentheses and proton numbering is depicted.

The peak observed at 63.94 ppm in **1** moves significantly upfield upon oxidation (Figure 4). It can thus be tentatively assigned to the proton closest to the formally oxidized metal centre, namely H(5) (see Scheme 4, top and middle). The assignment of the other protons was proposed in consideration of their distance to the magnetic centres.

Near-IR spectra: The spectrum of **1** in CH_3CN shows two broad, though relatively weak bands at 1186 nm (Figure 5), which are not observed in **2**. These two bands could therefore be assigned to an intervalence charge transfer (IVCT) system, characteristic of mixed-valence complexes. The position and intensity of these bands are not significantly modi-

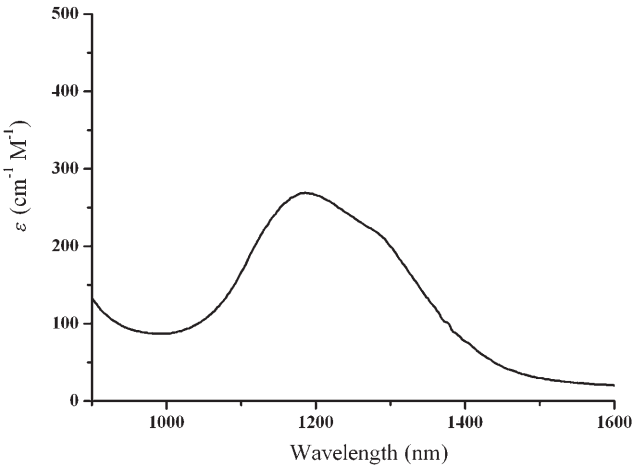

Figure 5. Near-IR spectrum of complex **1** in CH_3CN.

fied across a range of solvents including CH_2Cl_2, MeOH, and acetone. Even though the Hush formula[23] $H_{ab} = 0.0205\sqrt{\varepsilon_{max}\Delta\tilde{\nu}_{1/2}\tilde{\nu}_{max}}/r$ may not be used to interpret the spectra of these complexes, the appearance of these bands is consistent with a significant electronic interaction within the metal framework of **1**.[24] In accordance with the results of DFT calculations, the relatively weak intensity of these bands suggests that complex **1** could be tentatively assigned to Robin–Day class II of mixed-valent compounds.

Electrochemistry: In CH_2Cl_2, **1** exhibits three chemically reversible one-electron redox processes at $E_{1/2} = 0.16$, 0.46 and -0.59 V, constituting two oxidations and one reduction with respect to the starting redox state of **1** (Figure 6).

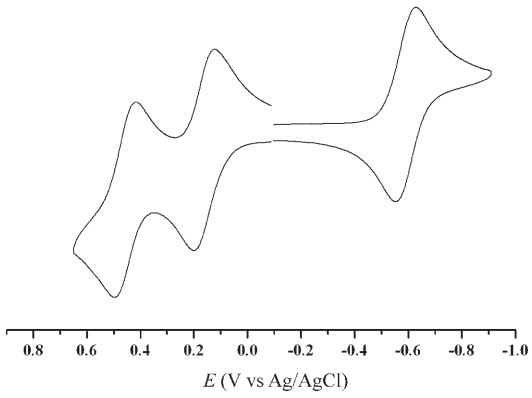

Figure 6. Cyclic voltammogram of compound **1** in CH_2Cl_2 containing 0.1 M TBAP with scan rate = 100 mV s^{-1}.

Assuming for **1** the formal oxidation model $(Ni_2)^{3+}$-Ni^{II}-$(Ni_2)^{3+}$ corresponding to a partial delocalization of the unpaired electron on each $\{Ni_2(napy)_4\}$ fragment, the first two processes are assigned to the successive oxidations of these fragments, eventually leading to complex **2**, symbolized as $[Ni^{II}$-Ni^{II}-Ni^{II}-Ni^{II}-$Ni^{II}]^{4+}$. The large difference ($\Delta E_{1/2} =$ 300 mV) between the potentials observed for the oxidation of the $(Ni_2)^{3+}$ moieties suggests the presence of a significant electron coupling between these fragments,[25] in accordance with the magnetic measurements and with the interpretation of the N-IR spectra.

DFT calculations: Calculations have been carried out on **1**, **2** and **5** to investigate, compare, and interpret the magnetic interactions in Ni_5 compounds. The geometries of all three complexes in the high-spin state were optimized with basis set 1 (BS1, see Experimental Section). The main geometrical parameters are displayed in Figure 2, with regard to the observed distances. The crystal structures are correctly reproduced by the calculations, except for a slight, but systematic overestimation of the distances, typical of hybrid or GGA functionals. This overestimation reaches 0.06 Å for some Ni–Ni distances and 0.09 Å for some Ni–Cl distances (Figure 2). In **1**, the remarkable shortening of the Ni(1)–Ni(2) distance with respect to **2**, leading to an unprecedented reversal with respect to the inner metal–metal distance, is correctly reproduced by the calculations (Figure 2). An optimization also carried out with BS1, but using the BP86 GGA functional yielded similar results.

Complex **5**, $[Ni_5(tpda)_4Cl_2]$, was taken as a benchmark test to calibrate, among the currently available standards, the exchange-correlation functional and the atomic basis sets most adequate to interpret the exchange coupling within the framework of the Heisenberg Hamiltonian and assuming two magnetic centres. As for $[Ni_3(dpa)_4Cl_2]$[8f] and $[Ni_4(Tsdpda)_4(H_2O)_2]$ (H_2Tsdpda = N-[p-toluenesulfonyl]dipyridyldiamine),[8g] the magnetic coupling occurs between the unpaired electrons of the terminal Ni atoms, both in high-spin state. The coupling therefore involves the superposition of two interactions: 1) an exchange mechanism along the metal chain involving the metal d_{z^2} orbitals and described by Cotton et al. as a spin polarization process,[5b] and 2) a superexchange along the pathways defined by the bridging ligands and involving the $d_{x^2-y^2}$-like orbitals of the terminal and of the internal metal atoms[8,10] (Scheme 4, top).

Even though somewhat different values have been proposed,[6a] the most reliable fit of the observed magnetic behaviour in **5** within the framework of the Heisenberg Hamiltonian corresponds to a J_{AB} value of -33.5 cm^{-1}.[1] Single-point calculations based upon the observed structure were carried out by Kitagawa et al. by using the B3LYP functional, the same formalism as in the present work, and all-electron basis sets of quality equivalent to BS2. The exchange coupling value obtained by Kitagawa et al. is -25.2 cm^{-1}. This corresponds to a remarkable agreement with the experimental value, given the well-documented sensitivity of J_{AB} to the geometrical parameters and to the calibration of the computational framework, especially concerning the exchange-correlation functional. The J_{AB} value calculated in the present work with BS2, with the geometry optimized with BS1, is only -13.2 cm^{-1}. Even though the difference is small in terms of energy, its importance regarding the order of magnitude of the calculated coupling requires an explana-

tion. Since the exchange-correlation functional and the spin-projection procedure are the same in both calculations, and the atomic basis sets display similar quality, the difference in the calculated J_{AB} value should be assigned to the molecular geometry, taken from the crystal structure in the work of Kitagawa et al.,[10] and optimized in the present study. The slight, but systematic overestimation of the calculated Ni–Ni distances, combined with the presence of a coupling linking the terminal nickel atoms along the metal chains gives credit to this assumption. Note that the J_{AB} values calculated by a similar procedure for Ni chain complexes with three and four atoms displaying a similar coupling between high-spin terminal atoms are also underestimated by a factor of ≈ 2.[8f,g] This is at variance with Cu chain complexes, which do not exhibit an exchange coupling through the metal chain.[8j]

With all nickel atoms in the oxidation state II, complex **2** is assumed to display the same type of coupling as **5**. This is confirmed by the DFT calculations, which assign in the HS state a spin population of 1.63 e to the terminal nickel atoms (Figure 2), completed to ≈ 2 e by the spin population of the chlorine (0.09 e) and of the surrounding nitrogen ligands (0.24 e altogether). In spite of this similarity, the fit of the magnetic susceptibility curve suggests a coupling intensity much reduced with respect to **5** ($J = -15.86\ cm^{-1}$). Accounting for the computational bias discussed above, this decrease of the coupling intensity is reproduced and even amplified by the calculations, which yield a J value of $-2.3\ cm^{-1}$ only. This strong decrease of $-J$ should be correlated with the drop of the spin population on Ni(2) from $+0.059$ e in **5** to $+0.022$ e in **2** (Figure 2).

The electron distribution and the magnetism in the reduced complex **1** should be interpreted with much caution. The formal, fully localized scheme of the reduction process, derived from the electronic structure of **2**, assumes the two incoming electrons to be accommodated in the x^2-y^2 orbital of the Ni(2) atoms, which are coordinated to the inner part of the naphthyridyl ligands (Scheme 4, middle). These metal atoms are therefore assigned the formal oxidation state I. This localized interpretation of mixed valency is, however, challenged by the experimental and theoretical analysis of complexes $[Ni_2(napy)_4(X_2)]^+$ (X = Cl, Br, I), which assess a fast mobility of the unpaired electron resulting in an assignment of these complexes to class III Robin–Day materials.[13,14] It should be noted first that the spin distribution of the unpaired electron in $[Ni_2(napy)_4(X_2)]^+$ calculated by means of the time-independent Schrödinger equation is fully delocalized between the magnetic centres due to molecular symmetry,[14] which represents a necessary though nonsufficient condition for an assignment to class III. The spin distribution deduced from the present calculations shows that this condition is not fulfilled anymore in the naphthyridyl fragments of **1**. The spin distribution is 1.445 e on the terminal Ni(1) centres (1.71 e including the ligand environment) versus 1.167 e (1.37 e) on Ni(2) (Figure 2). This distribution is practically half-way between the localized distribution proposed in Scheme 4 (top and middle: two unpaired electrons on Ni(1) and one on Ni(2), including the contribution from the coordination sphere), and a fully delocalized distribution (1.5 unpaired electrons on each magnetic centre). It appears from a more detailed analysis (Table 2) that this partial delocalization occurs along the metal axis through a transfer of the σ electron density from Ni(2) to Ni(1) in **1**, which corresponds to a shift of the spin density in the opposite direction (Table 2, Scheme 4, bottom). On the one hand, this delocalization, even partial, tends to create a three-electron two-centre Ni–Ni σ bond across each naphthyridyl fragment.[14] This is at variance with the fully localized scheme that prevails in complex **2** and in other $[Ni_5]^{10+}$ systems, and explains the remarkable contraction of the Ni(1)–Ni(2) distances, making it shorter than Ni(2)–Ni(3). On the other hand, the delocalization is not complete over the naphthyridyl fragments, because of their unsymmetrical environment along the chain axis, and even assuming a certain mobility of the unpaired electron, the $\{Ni_2(napy)_4\}$ moieties inserted in **1** cannot therefore be assimilated to their free, symmetrical counterpart. The question of the magnetic behaviour inside each $\{Ni_2(napy)_4\}$ fragment therefore requires to be re-examined in the environment of the $[Ni_5]^{8+}$ metal chain. To our knowledge, this represents the first molecular system in which a magnetic interaction is postulated between two mixed-valence fragments that should be themselves interpreted within the double-exchange framework.[20] A comprehensive treatment of this problem is far beyond the possibilities of Noodleman's broken-symmetry approach[26] and therefore exceeds the scope of the present work. As was done for the interpretation and fit of the temperature-dependent magnetic susceptibility curve, we have assumed complex **1** to be composed of two single magnetic centres with $S = 3/2$ corresponding each to a fully delocalized $[Ni_2]^{3+}$ moiety. The broken-symmetry singlet state is found to be $15.1\ cm^{-1}$ lower than the high-spin septet state, which corresponds after spin projection to a coupling constant J_{AB} of $-3.35\ cm^{-1}$ between the two $[Ni_2]^{3+}$ magnetic centres, underestimated by an order of magnitude with respect to the value deduced from the susceptibility curve ($J = -34.03\ cm^{-1}$). Calculated spin-density distribution suggests that the magnetic exchange coupling is quenched by the lack of 3d density at the central nickel: the overall spin density at Ni(3) is even negative (-0.051 e) due to the contribu-

Table 2. Detail of the gross atomic spin orbital populations (α spin–β spin, electrons; Mulliken analysis) calculated for the high-spin states of complexes **1** and **2** with BSI.

	$[Ni_5(bna)_4(Cl)_2]^{2+}$ (**1**)			$[Ni_5(bna)_4(Cl)_2]^{4+}$ (**2**)		
	σ[a]	δ[b]	others	σ[a]	δ[b]	others
Ni(1)[c]	0.60	0.83	0.015	0.72	0.80	0.11
Ni(2)	0.35	0.82	−0.01	0.07	0.02	−0.06
Ni(3)	0.06	0.01	−0.12	0.02	0.002	−0.006

[a] d_{z^2} spin population. [b] $d_{x^2-y^2}+d_{xy}$ spin population. [c] Ni(1): terminal position; Ni(2) : intermediate position; Ni(3): central position (Figure 1 and Scheme 4, bottom).

tion of the s and p functions. However, the lack of consistency between the experimental and the calculated results further questions the validity of the spin delocalization hypothesis within the fragments. A deeper investigation of the magnetism in **1**, or in an appropriate model of **1**, is clearly needed.

Single molecular conductance of $[Ni_5(bna)_4(NCS)_2][NCS]_2$ (3) and $[Ni_5(tpda)_4(NCS)_2]$ (4): To study the single molecular conductance of this new mixed-valence pentanickel complex, the axial isothiocyanate-substituted derivative compound **3** (Figure 7) was synthesized and isolated successfully.

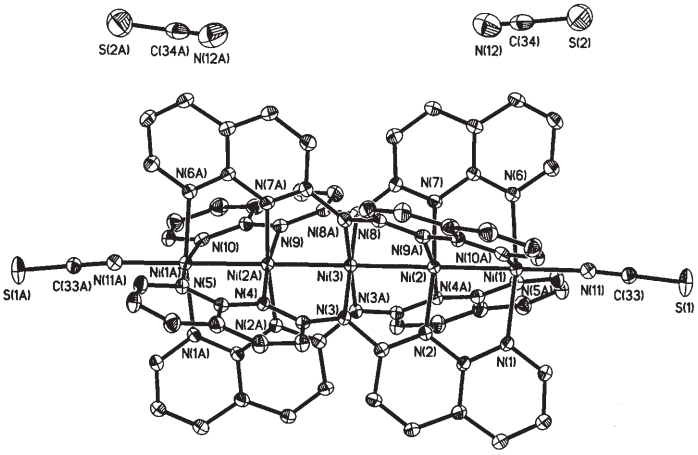

Figure 7. Molecular structure of complex **3**. Ellipsoids are drawn at 30% probability level. Hydrogen atoms and interstitial solvents have been omitted for clarity.

The physical properties of compound **3** are very similar to those of compound **1** (see Experimental Section and Supporting Information). It might therefore be assumed that unpaired electrons are partly delocalized in the $\{Ni_2(napy)_4\}$ moieties of **3** as they are in **1**. Measuring single molecular conductance by the STM break-junction method requires the molecules to have an anchoring group that can adsorb on the electrodes at which a bias voltage (E_{bias}) is applied and the conducting current is monitored. Because of the reasonable affinity between gold and isothiocyanate,[27] compound **3** and its $(Ni_5)^{10+}$ homologue **4**, were axially coordinated with isothiocyanate, and the measurements were carried out with a gold surface and a gold STM tip as electrodes. DFT/UB3LYP studies carried out on $[Ni_5(tpda)_4Cl_2]$ (**5**), the prototype of pentanickel EMACs, by Kitagawa et al.[10] and in the present work agree to conclude that the sole interaction occurring along the metal string is the weak antiferromagnetic interaction connecting the terminal nickel atoms. A previous extended Hückel study carried out on compound **4** also shows a zero-bond order between the nickel atoms.[15] Therefore, the difference in the conductance between **3** and **4** will be employed to gauge how the two-electron reduction of the pentanickel string affects the metal–metal interactions. Crystallization of $[Ni_5(bna)_4(NCS)_2][NCS]_4$ was unsuccessful and, thus, no attempt could be made to measure the conductance of this oxidized form.

The left-hand panels of Figure 8 display a few typical conductance traces for compounds **3** and **4**. The vertical axes

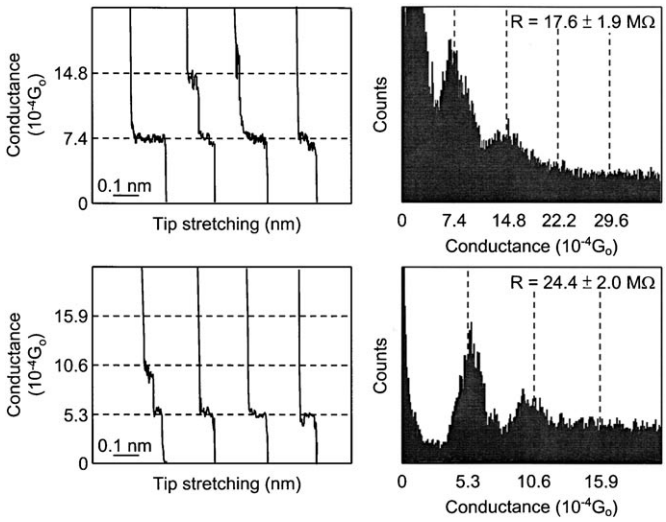

Figure 8. Conductance of a single molecule of $[Ni_5(bna)_4(NCS)_2][NCS]_2$ (upper panels) and $[Ni_5(tpda)_4(NCS)_2]$ measured by STM break-junction method. The curves are typical current–distance traces acquired upon stretching the molecular junctions. The traces are presented with arbitrary x axis offsets. The vertical axes represent conductance, calculated from the measured currents divided by the corresponding G_0 and E_{bias}, which are 30 and 50 mV for these traces, respectively, for compounds **3** and **4**. The conductance histograms have been obtained from more than 1000 measurements.

are plotted against G_0 ($=2e^2/h$, $\approx(12.9\,k\Omega)^{-1}$), which is the conductance quantum measured when the cross-section of a metallic contact is only that of a single gold atom.[28–30,28] The conductance values are converted from the electric current occurring while the STM tip is pulled away from the substrate. The traces are obtained by holding E_{bias} at 30 and 50 mV for compounds **3** (upper panel) and **4**, respectively. The sharp decrease associated with the tip stretching suggests a loss of molecules from the tip–substrate junction. The current values at the step are scaled with E_{bias}. Controlled experiments in blank toluene yield exponential tunnelling decay,[28,35] confirming that the staircase waveforms arise from compounds **3** and **4**.

The histograms at the right-hand panels are summarized from thousands of measurements and are plotted against G_0. The local maxima of occurrences are distributed as integer multiples of the fundamental ones, suggesting that the number of molecules in the junctions is one, two, and so forth.[29,30] The conductance and resistance for single molecules of compound **3** are $7.4\pm0.7\,G_0$ and $17.6\pm1.9\,M\Omega$, respectively, compared to $5.3\pm0.4\,G_0$ and $24.4\pm2.0\,M\Omega$ for compound **4**. The conductivity of **3** therefore appears higher by $\approx40\%$ than that of **4**, which is characterized in the first approximation by a zero-bond order between successive Ni^{II} atoms. This result supports the scheme of some electron delocalization along both Ni^{II}–Ni^{I} pairs.

Conclusions

The availability of binaphthyridylamide (bna) as a pentadentate ligand has led to the synthesis and characterization of a series of novel linear chain complexes of nickel containing five metal atoms. These complexes are closely related to the already large family of nickel polypyridylamides with which they share the helical shape of the ligand coating and a marked propensity to attach axial ligands at both ends of the metal chain. As far as the electronic structure is concerned, complex **2** exhibits the $[Ni_5]^{10+}$ metal core typical of $[Ni_5(tpda)_4Cl_2]$ (**5**) and related pentanickel chain complexes. As in other nickel chains, the new complex exhibits an antiferromagnetic interaction connecting the Ni^{II} atoms located at both ends of the chain, which are promoted to high spin because of their square-pyramidal coordination environment. At variance with the polypyridylamide complexes, which are usually neutral, complex **2** supports a charge of $4+$ in relation with the monoanionic character of the bna ligand. The magnetic coupling in **2** is found significantly weaker than in **5**. An important characteristic of this family of complexes is the accessibility of a stable, reduced form corresponding to a $[Ni_5]^{8+}$ metal core, still unprecedented in the collection of pentametallic chain complexes. In the reduced complex **1**, as in the other $[Ni_5]^{8+}$ complex **3** characterized in the present work, the extra pair is shared between the $\{Ni_2(napy)_4\}$ moieties, but the unsymmetrical environment of these fragments in the complex prevents a full delocalization of the mobile electron, as in $[Ni_2(napy)_4X_2]^+$. Near-IR spectroscopy and DFT calculations agree to suggest that both $\{Ni_2(napy)_4\}$ fragments in **1** could be considered as mixed-valent bimetallics and assigned to Robin–Day class II materials. Electrochemical measurements and the N-IR spectra can be interpreted in favour of a strong magnetic coupling between these fragments. A fit of the magnetic susceptibility curve by means of the usual Heisenberg Hamiltonian assuming a coupling between two fully delocalized magnetic centres yields a relatively strong exchange constant $J=-34\ cm^{-1}$. However, DFT calculations based upon similar assumptions failed to confirm such a large order of magnitude, and the lack of an appropriate model describing the coupling between two fragments subject to double-exchange leaves the question open to further investigation. Finally, one of the ultimate goals of the current interest towards nanowires, namely nanoelectronics, has been approached in a practical way by means of measurements of the single-molecular conductance of $[Ni_5(bna)_4(NCS)_2][NCS]_2$ (**3**) and $[Ni_5(tpda)_4(NCS)_2]$ (**4**) by the STM break-junction method. The reduced, $[Ni_5]^{8+}$ complex **3** was found more conductive by about 40% than the standard $[Ni_5]^{10+}$ compound **4**, which provides the first evidence that nickel-chain complexes could possibly approach the high conductance values previously reported for cobalt or chromium wires.[3]

Experimental Section

Materials: All reagents and solvents were purchased from commercial sources and were used as received unless otherwise noted. The precursors, 2-amino-1,8-naphthyridine and 2-chloro-1,8-naphthyridine were prepared according to the literature procedures.[31]

Binaphthyridylamine (Hbna): 2-Amino-1,8-naphthyridine (1.45 g, 10 mmol), 2-chloro-1,8-naphthyridine (1.64 g, 10 mmol), *t*BuOK (1.12 g 10 mmol), $[Pd_2(dba)_3]$ (0.91 mg 0.1 mmol) and dppp (82 mg, 0.2 mmol) were placed in a flame-dried flask under argon. The mixture was stirred and refluxed in THF (100 mL) for 72 h. The solvent was removed under reduced pressure. The mixture was washed by water and the precipitate was extracted by CH_2Cl_2 to obtain light yellow product. Yield: 1.97 g, 72%; ^{1}H NMR (400 MHz; [D]DMSO): $\delta=11.00$ (s, 1H), 8.91 (dd, $J=$ 5.97, 2.28 Hz, 2H), 8.34 (m, 6H), 7.43 ppm (dd, $J=12.23$, 3.56 Hz, 2H); MS(FAB): m/z: 274 $[M+H]^+$.

$[Ni_5(bna)_4(Cl)_2][PF_6]_2$ (1): A mixture of Hbna (273 mg, 1 mmol), naphthalene (50 g), and $NiCl_2$ (161 mg, 1.25 mmol) was placed in an Erlenmeyer flask. The mixture was heated (about 200 °C) for 15 h. A solution of *t*BuOK (112 mg, 1 mmol) in *n*-butanol (10 mL) was added dropwise. The solution then turned to dark green. The mixture was heated for another 10 h, cooled to about 70 °C, and treated with hexane to precipitate the metal complexes. The precipitate was washed with hexane to remove the residual naphthalene. The metal complex was extracted with CH_2Cl_2 (500 mL), and treated with KPF_6 (92 mg, 0.5 mmol) in CH_2Cl_2 (50 mL). The resulting solution was stirred for a week and dried under vacuum. The solid was extracted with CH_2Cl_2 and layered with hexane. After one week, deep green crystals were obtained. Yield: 261 mg, 60%; ^{1}H NMR (400 MHz; CD_3CN): $\delta=23.69$ (4H), 28.92 (4H), 32.54 (4H), 61.96 (4H), ca. 110 ppm (very broad peak); MS(MALDI): m/z: 1454 $[Ni_5(bna)_4(Cl)_2+H]^+$; UV/Vis (CH_3CN): $\lambda_{max}(\varepsilon)=316$ (4.72), 395 (9.01), 686 nm ($1.03\ 10^4\ M^{-1}cm^{-1}$).

$[Ni_5(bna)_4(Cl)_2][PF_6]_4$ (2): $[FeCp_2][PF_6]$ (130 mg, 0.396 mmol) was added to a solution of compound **1** (174 mg, 0.099 mmol) in CH_2Cl_2 (500 mL) under argon atmosphere. The red powder came out after the solution was stirred overnight. The mixture then was filtered. The remaining solid was dissolved in CH_3CN. Red crystals were obtained by slow diffusion of diethyl ether into this solution. Yield: 125 mg 63%; ^{1}H NMR (400 MHz; CD_3CN): $\delta=7.60$ (4H), 9.08 (4H), 23.5 (4H), 26.2 (4H), ca. 90 (very broad peak); MS(MALDI): m/z: 1454 $[Ni_5(bna)_4(Cl)_2+H]^+$; UV/Vis (CH_3CN): $\lambda_{max}(\varepsilon)=265$ (7.76), 384 (17.34), 526 nm ($1.19\ 10^4\ M^{-1}cm^{-1}$).

$[Ni_5(bna)_4(NCS)_2][NCS]_2$ (3): NaNCS (32 mg, 0.396 mmol) was added to a solution of compound **1** (174 mg, 0.099 mmol) in CH_2Cl_2 (500 mL) under argon atmosphere. The resulting solution was stirred for a week and dried at vacuum. The solid was extracted with CH_2Cl_2 (500 mL) and layered with hexane. After one week, deep green crystals were obtained. Yield: 134 mg, 84%; ^{1}H NMR (400 MHz, CD_3CN): $\delta=23.23$ (4H), 29.19 (4H), 32.95 (4H), 62.12 (4H), ca. 110 (very broad peak); MS(MALDI): m/z: 1499 $[Ni_5(bna)_4(NCS)_2+H]^+$; UV/Vis (CH_3CN): $\lambda_{max}(\varepsilon)$: 314 (4.52), 394 (9.66), 674 nm ($0.96\ 10^4\ M^{-1}cm^{-1}$).

$[Ni_5(tpda)_4(SCN)_2]$ (4): Compound **4** was synthesized according to our previous report[16] and used in STM studies.

Physical measurements: Magnetic susceptibility data were collected on a Quantum external magnetic field 3000G instrument. FAB mass spectra were taken on a JEOL HX-110 HF double-focusing spectrometer operating in the positive ion detection mode. The MALDI spectra were performed on a MALDI-TOF mass spectrometer Voyager DE-STR. ^{1}H NMR spectra for organic and inorganic complexes were recorded in DMSO and CD_3CN with a Bruker AMX 400 MHz spectrometer. Electronic spectra of **1**, **2**, and **3** in CH_3CN were measured in a range of 250–2500 nm on a Perkin–Elmer Lambda 900 UV-Vis-NIR Spectrometer. Electrochemistry was carried out on a CH instrument (Model 750 A), using CH_2Cl_2 solvent with 0.1 M TBAP and 1 mM analytes. Cyclic voltammetry was recorded with a home-made three-electrode cell equipped with a BAS glassy carbon (0.07 cm^2) disk as the working electrode, a platinum wire as the auxiliary electrode, and a home-made Ag/AgCl (saturated) reference electrode. The reference electrode was separated from

the bulk solution by a double junction filled with electrolyte solution. Potentials are reported versus Ag/AgCl (saturated) and referenced to the ferrocene–ferrocenium ($[Cp_2Fe]/[Cp_2Fe]^+$) couple which occurs at $E_{1/2} = +0.54$ V versus Ag/AgCl(saturated). The working electrode was polished with 0.03 μm alumina on Buehler felt pads and was subjected to ultrasound for 1 min prior to each experiment. The reproducibility of individual potential values was within ±5 mV.

X-ray structure determinations: Crystallographic data were collected at 150(1 K on a NONIUS Kappa CCD diffractometer with graphite-monochromatized $Mo_{K\alpha}$ radiation ($\lambda = 0.71073$ Å). Cell parameters were retrieved and refined with DENZO-SMN software on all observed reflections. Data reduction was performed with the DENZO-SMN software.[32] An empirical absorption was based on the symmetry-equivalent reflection and absorption corrections were applied with the SORTAV program.[33] All the structures were solved and refined with the SHELX-97 programs.[34] The hydrogen atoms were included in calculated positions and refined with a riding mode.

STM measurement: The experimental procedures and data treatment for STM (scanning tunnelling microscopy) break-junction method were documented in detail by the groups of Tao and Lindsay.[35,36] Briefly, the experiments were carried with a NanoScope IIIa controller (Veeco, Santa Barbara, CA). A gold STM tip was brought into and out of contact with a gold substrate in toluene (TEDIA) containing 1 mM compound **3** or **4** and housed in a dry N_2(g)-filled chamber. Upon the repeated formation of the tip–substrate gap, the isothiocyanate headgroups at the termini of the EMACs bind to the gold electrodes and complete a molecular junction. The current-to-tip stretching profiles were recorded by a NanoScope built-in program and exported as ASCII files, which subsequently were used to plot the frequency histograms of the molecular conductance by Origin (version 6.0, Microcal Software).

Substrates for STM experiments were 100 nm-thick gold films thermally evaporated onto glass slides pre-deposited with a 5 nm Cr adhesive layer (99.99%, Super Conductor Materials, Suffern, NY). The vacuum pressure was nominally 2×10^{-6} Torr. Prior to placing the glass slide in the bell-jar evaporator (Auto 306, Edwards High Vacuum International, West Sussex, UK), the glass slides were cleaned with piranha solution, rinsed thorough with copious deionised water, and oven-dried in 1 hr. The piranha solution is a 1:3 (v/v) mixture of 30% H_2O_2 and concentrated H_2SO_4, which *reacts violently with organics and should be handled with great care*.

DFT calculations: Calculations and geometry optimizations on **1**, **2** and **5** were carried out by using the density functional theory (DFT) formalism with the spin unrestricted option, as implemented in the Gaussian03 software,[37] with the B3LYP and with the BP86 exchange-correlation functionals. Two sets of atomic basis sets, referred to as BSI and BSII, were used. In BSI, all-electron valence double-ζ basis sets (D95 V) were used to describe C, N, and H atoms. Then, Los Alamos core potentials were used to model the neon cores of Cl and Ni, whereas the valence shell of these atoms was described at the double-ζ level (LanL2DZ basis). In BSII, all atoms were described with all-electron 6–31G basis sets. For Ni and Cl, the standard 6–31G basis was supplemented with diffuse functions (exponents for Ni: 0.128529 and 0.045195 for the s and p shells; 0.2 for the d shell; Cl: 0.142657 and 0.0483 for both the s and the p shells) and one d-type (exponent 0.75 for Cl) or f-type (exponent 0.8 for Ni) polarization functions. BSI was used for all geometry optimizations and for the Mulliken spin populations. The exchange coupling constant J_{AB} was then determined by means of single-point calculations carried out with BSII on the high-spin (HS) and broken-symmetry (BS) states of all three systems, as explained below, by using the geometry optimized with BSI for the HS state.

The antiferromagnetic low-spin state of **1** and **2** was characterized and its geometry optimized by using the broken symmetry (BS) approach first proposed by Ginsberg,[38] and then developed by Noodleman.[26] The exchange parameter $2J_{AB}$ between two magnetic centres A and B is defined by the Heisenberg–Dirac–van Vleck (HDVV) Hamiltonian [Eq. (2)]

$$\hat{H}^{HDVV} = -J_{AB}\hat{S}_A \cdot \hat{S}_B \quad (2)$$

Complexes **1**, **2**, and **5** were assumed to behave as complexes with two magnetic centres. In **2** and **5**, the magnetic centres were located on the terminal metals and extend toward the four equatorial nitrogen ligands. They were assigned each a total spin of 1. In complex **1**, the whole $\{Ni_2(napy)_4\}$ moieties were considered each as a unique magnetic centre, delocalized over the two metal atoms, and partly over the nitrogen ligands. Each delocalized magnetic centre was assigned a total spin of 3/2. Since the broken-symmetry solutions are not proper eigenvalues of $\hat{S}^2$, but a weighted average of the energies of the pure spin multiplets, an approximate projection technique was employed, as proposed and used by Yamaguchi et al. [Eq. (3)] within the ab initio or the DFT frameworks:[39] in which $^{HS}\langle S^2\rangle$ and $^{BS}\langle S^2\rangle$ denote the total spin angular momentum calculated in the high-spin and in the broken-symmetry solutions, respectively.

$$J_{AB} = 2(^{BS}E - ^{HS}E)/(^{HS}\langle S^2\rangle - ^{BS}\langle S^2\rangle) \quad (3)$$

Acknowledgements

The authors acknowledge the CNRS, the Ministère de l'Education Nationale, de l'Enseignement Supérieur et de la Recherche (MENESR, Paris, France), and the National Science Council and the Ministry of Education of Taiwan for financial support. Calculations have been shared between the IDRIS (CNRS, Orsay, France), the CINES (Montpellier, France), and the NCHC (Taiwan) computer centres. We thank Jung-Che Chang, Shang-Shin Lo, Long-An Li, and Professor Chen-Yu Yeh for their help concerning electrochemistry.

[1] a) J. F. Berry, F. A. Cotton, P. Lei, T. Lu, C. A. Murillo, *Inorg. Chem.* **2003**, *42*, 3534; b) F. A. Cotton, L. M. Daniels, T. Lu, C. A. Murillo, X. Wang, *J. Chem. Soc. Dalton Trans.* **1999**, 517.

[2] a) L.-G. Zhu, S.-M. Peng, *Wuji Huaxue Xuebao* **2002**, *18*, 117; b) J. K. Bera, K. R. Dunbar, *Angew. Chem.* **2002**, *114*, 4633; *Angew. Chem. Int. Ed.* **2002**, *41*, 4453.

[3] a) S.-Y. Lin, I-W. P. Chen, C.-h. Chen, M.-H. Hsieh, C.-Y. Yeh, T.-W. Lin, Y.-H. Chen, S.-M. Peng, *J. Phys. Chem. B* **2004**, *108*, 959; b) D.-H. Chae, J. F. Berry, S. Jung, F. A. Cotton, C. A. Murillo, Z. Yao, *Nano Lett.* **2006**, *6*, 165; c) I-W. P. Chen, M.-D. Fu, W.-H. Tseng, J.-Y. Yu, S.-H. Wu, C.-J. Ku, C.-h. Chen, S.-M. Peng, *Angew. Chem.* **2006**, *118*, 5946; *Angew. Chem. Int. Ed.* **2006**, *45*, 5814.

[4] a) J. F. Berry, in *Multiple Bonds between Metal Atoms*, 3rd ed. (Eds.: F. A. Cotton, C. A. Murillo, R. A. Walton), Springer, New York, **2005**; b) C.-Y. Yeh, C.-C. Wang, C.-h. Chen, S.-M. Peng, in *Nano Redox Sites: Nano-Space Control and its Applications* (Ed.: T. Hirao), Springer, Berlin, **2006**, Chapter 5, pp. 85–117.

[5] a) F. A. Cotton, L. M. Daniels, C. A. Murillo, I. Pascual, *J. Am. Chem. Soc.* **1997**, *119*, 10223; b) J. F. Berry, F. A. Cotton, C. A.; Murillo, *Dalton Trans.* **2003**, 3015; Murillo, *Dalton Trans.* **2003**, 3015; c) J. F. Berry, F. A. Cotton, L. M. Daniels, C. A. Murillo, X. Wang, *Inorg. Chem.* **2003**, *42*, 2418; d) F. A. Cotton, C. A. Murillo, X. Wang, *Inorg. Chem.* **1999**, *38*, 6294; e) J. F. Berry, F. A. Cotton, T. Lu, C. A. Murillo, B. K. Roberts, X. Wang, *J. Am. Chem. Soc.* **2004**, *126*, 7082; f) R. Clérac, F. A. Cotton, L. M. Daniels, K. R. Dunbar, K. Kirschbaum, C. A. Murillo, A. A. Pinkerton, A. J. Schultz, X. Wang, *J. Am. Chem. Soc.* **2000**, *122*, 6226; g) R. Clérac, F. A. Cotton, K. R. Dunbar, C. A. Murillo, I. Pascual, X. Wang, *Inorg. Chem.* **1999**, *38*, 2655; h) J. F. Berry, F. A. Cotton, C. A. Murillo, B. K. Roberts, *Inorg. Chem.* **2004**, *43*, 2277; i) J. F. Berry, F. A. Cotton, C. S. Fewox, T. Lu, C. A. Murillo, X. Wang, *Dalton Trans.* **2004**, 2297; j) D. W. Armstrong, F. A. Cotton, A. G. Petrovic, P. L. Polavarapu, M. M. Warnke, *Inorg. Chem.* **2007**, *46*, 1535.

[6] a) S.-M. Peng, C.-C. Wang, Y.-L. Jang, Y.-H. Chen, F.-Y. Li, C.-Y. Mou, M.-K. Leung, *J. Magn. Magn. Mater.* **2000**, *209*, 80; b) C.-H. Yeh, C.-H. Chou, K.-C. Pan, C.-C. Wang, G.-H. lee, Y. O. Su, S.-M. Peng, *J. Chem. Soc. Dalton Trans.* **2002**, 2670; c) C.-Y. Yeh, G.-H. Lee, S.-M. Peng, *Inorg. Chem.* **2002**, *41*, 4096; d) T.-B. Tsao, G.-H.

Lee, C.-Y. Yeh, S.-M. Peng, *Dalton Trans.* **2003**, 1465; e) C.-H. Chien, J.-C. Chang, C.-Y. Yeh, L.-M. Fang, Y. Song, S.-M. Peng, *Dalton Trans.* **2006**, 3249; f) C.-H. Chien, J.-C. Chang, C.-Y. Yeh, G.-H. Lee, L.-M. Fang, S.-M. Peng, *Dalton Trans.* **2006**, 2106; g) M.-Y. Huang, C.-Y. Yeh, G.-H. Lee, S.-M. Peng, *Dalton Trans.* **2006**, 5683.

[7] T. Sheng, R. Appelt, V. Comte, H. Vahrenkamp, *Eur. J. Inorg. Chem.* **2003**, 3731.

[8] a) M.-M. Rohmer, M. Bénard, *J. Am. Chem. Soc.* **1998**, *120*, 9372; b) M.-M. Rohmer, A. Strich, M. Bénard, J.-P. Malrieu, *J. Am. Chem. Soc.* **2001**, *123*, 9126; c) N. Benbellat, M.-M. Rohmer, M. Bénard, *Chem. Commun.* **2001**, 2368; d) M.-M. Rohmer, M. Bénard, *Chem. Soc. Rev.* **2001**, *30*, 340; e) M.-M. Rohmer, M. Bénard, *J. Cluster Sci.* **2002**,*13*, 333; f) P. Kiehl, M.-M. Rohmer, M. Bénard, *Inorg. Chem.* **2004**, *43*, 3151; g) X. López, M.-Y. Huang, G.-C. Huang, S.-M. Peng, F.-Y. Li, M. Bénard, M.-M. Rohmer, *Inorg. Chem.* **2006**, *45*, 9075; h) X. López, M. Bénard, M.-M. Rohmer, *J. Mol. Struct. THEOCHEM* **2006**, *777*, 53; i) X. López, M. Bénard, M.-M. Rohmer, *Inorg. Chem.* **2007**, *46*, 5; j) M. Bénard, J. F. Berry, F. A. Cotton, C. Gaudin, X. López, C. A. Murillo, M.-M. Rohmer, *Inorg. Chem.* **2006**, *45*, 3932.

[9] D. A. Pantazis, J. E. McGrady, *J. Am. Chem. Soc.* **2006**, *128*, 4128.

[10] Y. Kitagawa, M. Shoji, K. Koizumi, T. Kawakami, M. Okumura, K. Yamaguchi, *Polyhedron* **2005**, *24*, 2751.

[11] M. B. Robin, P. Day, *Adv. Inorg. Chem. Radiochem.* **1967**, *10*, 247.

[12] *Mixed Valence Compounds* (Ed.: D. M. Brown), Reidel, Dordrecht (The Netherlands), **1980**.

[13] a) D. Gatteschi, C. Mealli, L. Sacconi, *J. Am. Chem. Soc.* **1973**, *95*, 2736; b) L. Sacconi, C. Mealli, D. Gatteschi, *Inorg. Chem.* **1974**, *13*, 1985; c) A. Bencini, D. Gatteschi, L. Sacconi, *Inorg. Chem.* **1978**, *17*, 2760.

[14] A. Bencini, E. Berti, A. Caneschi, D. Gatteschi, E. Giannasi, I. Invernizzi, *Chem. Eur. J.* **2002**, *8*, 3660.

[15] S.-J. Shieh, C.-C. Chou, G.-H. Lee, C.-C. Wang, S.-M. Peng, *Angew. Chem.* **1997**, *109*, 57; *Angew. Chem. Int. Ed. Engl.* **1997**, *36*, 56.

[16] C.-C. Wang, W.-C. Lo, C.-C. Chou, G.-H. Lee, J.-M. Chen, S.-M. Peng, *Inorg. Chem.* **1998**, *37*, 4059.

[17] The structural environment of Ni(1) in **2** is also quite similar to that of Ni in the series of binuclear, mixed-valent complexes $[Ni_2(napy)_4X_2]^+$ (X = Cl, Br, I) (see ref. [14]).

[18] a) P. A. M. Dirac, *Proc. R. Soc. London Ser. A* **1926**, *112*, 661; **1929**, *123*, 714; b) W. Heisenberg, *Z. Phys.* **1926**, *38*, 411; c) J. H. van Vleck, *Theory of Electric and Magnetic Susceptibilities*, Oxford University Press, London, **1932**.

[19] For two equivalent magnetic centres with $S_1 = S_2 = 1$, the van Vleck equation can be developed as $\chi = \frac{Ng^2\beta^2}{kT}\frac{2\exp(J/kT)+10\exp(3J/kT)}{1+3\exp(J/kT)+5\exp(3J/kT)}$, in which N is Avogadro's constant, g is the Landé factor, β is the Bohr magneton, k is the Boltzmann constant, and T is temperature. When $S_1 = S_2 = 3/2$, the development as a function of the same quantities becomes $\chi = \frac{Ng^2\beta^2}{kT}\frac{2\exp(J/kT)+10\exp(3J/kT)+28\exp(6J/kT)}{1+3\exp(J/kT)+5\exp(3J/kT)+7\exp(6J/kT)}$.

[20] a) C. Zener, *Phys. Rev.* **1951**, *82*, 403; b) P. W. Anderson, H. Hasegawa, *Phys. Rev.* **1955**, *100*, 675; c) G. Blondin, J.-J. Girerd, *Chem. Rev.* **1990**, *90*, 1359.

[21] The peaks at 107 ppm of **1** and 92.5 ppm of **2** are too broad to be integrated.

[22] a) G. N. La Mar, G. R. Van Hecke, *Inorg. Chem.* **1970**, *9*, 1546; b) I. Bertini, D. Gatteschi, *Inorg. Chem.* **1973**, *12*, 2740; c) I. Berini, P. Turano, A. J. Vila, *Chem. Rev.* **1993**, *93*, 2833.

[23] a) N. S. Hush, *Prog. Inorg. Chem.* **1967**, *8*, 391; b) C. Creutz, *Prog. Inorg. Chem.* **1983**, *30*, 1; c) N. S. Hush, *Coord. Chem. Rev.* **1985**, *64*, 135.

[24] F. A. Cotton, C. Y. Liu, C. A. Murillo, Q. Zhao, *Inorg. Chem.* **2006**, *45*, 9493.

[25] S. Khanra, T. Weyhermuller, E. Bill, P. Chaudhu, *Inorg. Chem.* **2006**, *45*, 5911.

[26] a) L. Noodleman, *J. Chem. Phys.* **1981**, *74*, 5737; b) L. Noodleman, E. J. Baerends, *J. Am. Chem. Soc.* **1984**, *106*, 2316; c) L. Noodleman, E. R. Davidson, *Chem. Phys.* **1986**, *109*, 131; d) L. Noodleman, J. G. Norman, Jr., J. H. Osborne, A. Aizman, D. A. Case, *J. Am. Chem. Soc.* **1985**, *107*, 3418; e) L. Noodleman, D. A. Case, A. Aizman, *J. Am. Chem. Soc.* **1988**, *110*, 1001; f) L. Noodleman, C. Y. Peng, D. A. Case, J. M. Mouesca, *Coord. Chem. Rev.* **1995**, *144*, 199.

[27] M.-D. Fu, I-W. P. Chen, H.-C. Lu, C.-T. Kuo, W.-H. Tseng, C.-h. Chen, *J. Phys. Chem. C* **2007**, *111*, 11450.

[28] X. Li, J. He, J. Hihath, B. Xu, S. M. Lindsay, N. Tao, *J. Am. Chem. Soc.* **2006**, *128*, 2135.

[29] A. I. Yanson, G. Rubio-Bollinger, H. E. van den Brom, N. Agrait, J. M. van Ruitenbeek, *Nature*, **1998**, *395*, 783.

[30] H. Ohnishi, Y. Kondo, K. Takayanagi, *Nature*, **1998**, *395*, 780.

[31] a) C. Reichardt, W. Scheibelein, *Tetrahedron Lett.* **1977**, *18*, 2087; b) G. R. Newkome, S. J. Garbis, V. K. Majestic, F. R. Fronczek, G. Chiari, *J. Org. Chem.* **1981**, *46*, 833.

[32] Z. Otwinowski, W. Minor, *Methods Enzymol.* **1997**, *276*, 307.

[33] R. H. Blessing, *Acta Crystallogr. Sect. A* **1995**, *51*, 33.

[34] a) G. M. Sheldrick, *Acta Crystallogr. Sect. A* **1990**, *46* ,467; b) G. M. Sheldrick, SHELXL-97, Program for the Solution and Refinement of Crystal Structures, University of Göttingen, Germany, **1997**.

[35] B. Xu, N. J. Tao, *Science* **2003**, *301*, 1221 – 1223.

[36] X. Li, J. He, J. Hihath, B. Xu, S. M. Lindsay, N. Tao, *J. Am. Chem. Soc.* **2006**, *128*, 2135 – 2141.

[37] Gaussian 03 (Revision B.05), M. J. Frisch, G. W. Trucks, H. B. Schlegel, G. E. Scuseria, M. A. Robb, J. R. Cheeseman, J. A. Montgomery Jr., T. Vreven, K. N. Kudin, J. C. Burant, J. M. Millam, S. S. Iyengar, J. Tomasi, V. Barone, B. Mennucci, M. Cossi, G. Scalmani, N. Rega, G. A. Petersson, H. Nakatsuji, M. Hada, M. Ehara, K. Toyota, R. Fukuda, J. Hasegawa, M. Ishida, T. Nakajima, Y. Honda, O. Kitao, H. Nakai, M. Klene, X. Li, J. E. Knox, H. P. Hratchian, J. B. Cross, C. Adamo, J. Jaramillo, R. Gomperts, R. E. Stratmann, O. Yazyev, A. J. Austin, R. Cammi, C. Pomelli, J. W. Ochterski, P. Y. Ayala, K. Morokuma, G. A. Voth, P. Salvador, J. J. Dannenberg, V. G. Zakrzewski, S. Dapprich, A. D. Daniels, M. C. Strain, O. Farkas, D. K. Malick, A. D. Rabuck, K. Raghavachari, J. B. Foresman, J. V. Ortiz, Q. Cui, A. G. Baboul, S. Clifford, J. Cioslowski, B. B. Stefanov, G. Liu, A. Liashenko, P. Piskorz, I. Komaromi, R. L. Martin, D. J. Fox, T. Keith, M. A. Al-Laham, C. Y. Peng, A. Nanayakkara, M. Challacombe, P. M. W. Gill, B. Johnson, W. Chen, M. W. Wong, C. Gonzalez, J. A. Pople, Gaussian, Inc., Pittsburgh, PA, **2004**.

[38] A. P. Ginsberg, *J. Am. Chem. Soc.* **1980**, *102*, 111.

[39] For a recent review, see S. Yamanaka, R. Takeda, M. Shoji, Y. Kitagawa, H. Honda, K. Yamaguchi, *Int. J. Quantum Chem.* **2005**, *105*, 605.

Received: May 16, 2007
Published online: September 11, 2007

